Electronic Supplementary Material (ESI) for Soft Matter.
This journal is © The Royal Society of Chemistry 2024

Supplementary Materials

Tensile force field takes crucial roles in local invasion of tumor cells through a mechano-chemical coupling mechanism

Jianfeng Meng, Xiangyu Xu, Chaohui Jiang, Peng Xia, Pengfei Xu, Liangfei Tian, Yingke Xu, Dechang Li, Youhua Tan, Baohua Ji

Numerical methods

Coarse-grained model of tumor-ECM system

We utilized a coarse-grained (CG) modeling approach to simulate the interaction between tumor spheroids and ECM fibers, as depicted in Fig. 1S. Specifically, the CG model represented the membrane and cytoskeleton of a cell using CG particles, the interaction of which was modeled by bonded or nonbonded interaction (Fig. S1B). The bonded interactions modeling cell membrane tension and tensional force in the cytoskeletal were referred to as intracellular forces. The non-bonded interactions between neighboring cells, referred to as intercellular forces, can be disrupted and reformed once broken. These non-bonded interactions enable us to simulate the detachment of cells from the tumor and the long-distance migration of tumor cells (Fig. S1C&D). The cell structure may be deformed by its active contraction and external forces from neighboring cells within the system. Figure S1D highlights the intracellular and intercellular forces considered in the multi-cellular model system. In previous studies, the CG model was extensively utilized to examine the collective cell motion on the patterned surfaces and wound formation within a single cell layer when subjected to cyclic stretching.[1, 2]

The ECM fibers were also discretized using CG particles that are connected by bonded interactions. In addition, bonded interaction was used to model the crosslinking between/among fibers which allowed for the formation of a network (Fig. S1E). Density was adjustable and the orientation of the fibers in the network was randomly established.

The interaction between cells and ECM fibers is modeled by Lennard-Jones potential between particles of the cell and those of fibers within a distance threshold.

The driving force for cell migration is generated by the interaction force between cell and matrix fibers via focal adhesions, called cell traction force.[3] Both experiments and theories[4] indicate that the magnitude of traction force is governed by the so-called traction-distance law. Hence, the traction force depends on the cell's size and degree of polarization. For a polarized cell, the traction force is often simplified by a force dipole.[5, 6] The driving force is equal to the net traction force at the critical point of detaching of the cell rear.

In addition, we considered the cell area as constant; therefore, we applied area constraints on the cell. A cortex-like membrane is introduced at the boundary of the tumor spheroid to mimic the basement membrane (Fig. S1C). The cortex is usually formed cross multiple cells at the periphery, which constrict the tumor cells.[7-9]

In summary, each node in the model is subjected to multiple forces, including the intercellular force $\boldsymbol{F}_i^{inter}$, the intracellular force $\boldsymbol{F}_i^{intra}$, the active contraction force $\boldsymbol{F}_i^{active}$, the driving force of cell motion $\boldsymbol{F}_i^{driving}$, the area constraint force $\boldsymbol{F}_i^{area}$, the constraint force from the basement membrane $\boldsymbol{F}_i^{basement}$, and the cell traction force between cell and fiber $\boldsymbol{F}_i^{adhesion}$ (as depicted in Fig. 2D). The motion of CG particles indexed with i (where i =1…N) is governed by the Langevin equation[1, 2]

$$m_i \frac{d^2\boldsymbol{r}_i}{dt^2} = -m_i\gamma_i \frac{d\boldsymbol{r}_i}{dt} + \boldsymbol{F}_i^{Resultant}(\boldsymbol{r}) + \mathring{\boldsymbol{r}}_i(t) \tag{1}$$

where the resultant force on each node

$$\boldsymbol{F}_i^{Resultant}(\boldsymbol{r}) = \boldsymbol{F}_i^{intra}(\boldsymbol{r}) + \boldsymbol{F}_i^{inter}(\boldsymbol{r}) + \boldsymbol{F}_i^{area}(\boldsymbol{r}) + \boldsymbol{F}_i^{active}(\boldsymbol{r}) + \boldsymbol{F}_i^{basement}(\boldsymbol{r}) + \boldsymbol{F}_i^{driving}(\boldsymbol{r}) + \boldsymbol{F}_i^{adhesion}(\boldsymbol{r}) \tag{2}$$

and m_i represents the mass of the particle, while γ_i is the friction constant. The random force, which is represented by Gaussian white noise to account for the thermal fluctuations, is denoted by $\mathring{\boldsymbol{r}}_i(t)$.

$\mathbf{F}_i^{\text{intra}}(\mathbf{r})$ includes the intracellular force between particles in the membrane ($\mathbf{F}_i^{\text{membrane}}$) and those in the cytoskeleton ($\mathbf{F}_i^{\text{skeleton}}$) of one cell. The intracellular force between the CG particles in the membrane is described as $\mathbf{F}_i^{\text{membrane}} = \left(E_{\text{membrane}}\varepsilon_{ij}\right)\hat{\mathbf{r}}_{ij}$, $E_{\text{membrane}} = 9 \times 10^4\, pN/\mu m$ is the elasticity of the membrane.[1] $\mathbf{F}_i^{\text{skeleton}} = \sum_{j=1}^{M_i}\left(\mu_{skeleton}\frac{\partial \varepsilon_{ij}}{\partial t} + E_{skeleton}\varepsilon_{ij}\right)\hat{\mathbf{r}}_{ij}$ describes the intracellular force for particles in the cytoskeleton.[1] The parameters $\mu_{skeleton} = 0.3\, pN\, s/\mu m$ and $E_{skeleton} = 35\, pN/\mu m$ are the viscoelastic and the elastic coefficients of the skeleton, respectively.[10] ε_{ij} is the deformation between particles *i* and *j*, and $\hat{\mathbf{r}}_{ij}$ is the unit vector pointing from particles *i* to *j*.

$\mathbf{F}_i^{\text{inter}}$ represents the intercellular force between the CG particles at the cell boundaries, characterizing the cell-cell interaction. The force $\mathbf{F}_i^{\text{inter}}$ is comprised of the normal and shear components[11, 12]

$$f_i^n = \begin{cases} \sigma_c\left(\frac{r_{ij}^n-\delta_0}{\delta_{dn}-\delta_0}\right)e^{\left(1-\frac{r_{ij}^n-\delta_0}{\delta_{dn}-\delta_0}\right)} & r_{ij}^n \le \delta_{dn} \\ \sigma_c\frac{\delta_{fn}-r_{ij}^n}{\delta_{fn}-\delta_{dn}} & \delta_{dn} \le r_{ij}^n \le \delta_{fn} \\ 0 & \delta_{fn} \le r_{ij}^n \end{cases}; \quad f_i^t = \begin{cases} \tau_c\frac{r_{ij}^t}{\delta_{dt}}e^{\left(\frac{1}{2}-\frac{\left(r_{ij}^t\right)^2}{2\left(\delta_{dt}\right)^2}\right)} & r_{ij}^t \le \delta_{dt} \\ \tau_c\frac{\delta_{ft}-r_{ij}^t}{\delta_{ft}-\delta_{dt}} & \delta_{dt} \le r_{ij}^t \le \delta_{ft} \\ 0 & \delta_{ft} \le r_{ij}^t \end{cases} \tag{3}$$

where f_i^n and f_i^t represent the normal and shear intercellular forces, respectively. Additionally, the maximum values of f_i^n and f_i^t are denoted by the parameters σ_c and τ_c, respectively. According to previous studies, the parameters σ_c and τ_c were set to be 1100 $pN/\mu m^2$ and 550 $pN/\mu m^2$, respectively.[1, 2, 13] r_{ij}^n and r_{ij}^t are the normal and tangential distances between particles *i* and *j*, respectively. The equilibrium distance of the intercellular interaction is set as $\delta_0 = 0.5\mu m$. The critical lengths for the maximum values of f_i^n and f_i^t are $\delta_{dn} = 1\mu m$ and $\delta_{dt} = 1\mu m$, respectively. $\delta_{fn} = 2\mu m$ and $\delta_{ft} = 2\mu m$ are the cutoff lengths used to calculate the interaction forces.[1, 2]

The model explicitly incorporates $\mathbf{F}_i^{\text{active}}$ to account for the active contraction of the cell. Based on the traction-distance law and prior experimental findings, the tension force in the cell is approximately proportional to the distance from the cell edge to the cell center.[4] According to earlier studies, the tension force for a polarized cell can be modeled as a force dipole.[5, 6] In this

model, the active contraction force is described by $\mathbf{F}_i^{\text{active}} = k_d(\mathbf{r}_i - \mathbf{r}_{i0})$ based on the traction-distance law. The parameter $k_d = 10\, pN/\mu m$ characterizes the cell contraction strength,[4, 14] $\mathbf{r}_i$ represents particle *i's* position vector, and $\mathbf{r}_{i0}$ stands for the position vector of the cell center.[1, 2]

The force of the areal constraint is denoted by $\mathrm{F}_i^{\text{area}} = -\frac{k_a(A-A_0)}{A_0}\frac{\partial A}{\partial r_i}$. The constant of the areal constraint is represented by the parameter $k_a = 5 \times 10^4\, pN/\mu m$.[1, 2, 15] A_0 refers to the cell area in its original state. The cell area A of current state is determined by the Gauss's area formula which is given by $A = \frac{1}{2}[(x_1y_2 - x_2y_1) + (x_2y_3 - x_3y_2) + \cdots + (x_ny_1 - x_1y_n)]$. Here, x_i and y_i correspond to the ith particle's Cartesian coordinates in the cell membrane.

The imbalance of cell traction force during detachment of the cell rear generates the driving force for cell migration.[3] This is related to the degree of cell polarization and size. In this model, we describe the self-driving force for active cell migration as $\mathrm{F}_i^{\text{driving}} = k_{dv}L_{max}\ln(AR_i)$. Here, k_{dv} represents the intensity of the driving force of $1\, pN/\mu m$,[1] while L_{max} denotes the length of the cell's long axis, and *AR* reflects the cell's aspect ratio.

There is a transcellular structure formed at the edge of tumor cell spheroids, called the basement membrane, which restricts the cells from detaching from the tumor spheroids.[7] Using the eight-quadrant method, we dynamically identify new boundary points when some cells detach, and exclude the detached tumor cells during tumor invasion process. $\mathrm{F}_i^{\text{basement}}$ represents the restricting force exerted on the ith point on the membrane due to the bending of the basement membrane (Fig. S1C):

$$\vec{F}_i^{basement} = \mathrm{K}(cos\alpha - cos\alpha_0)\left[\frac{\vec{r}_{ik}}{r_{ij}r_{ik}} + \frac{\vec{r}_{ij}}{r_{ij}r_{ik}} - cos\theta\left(\frac{\vec{r}_{ij}}{r_{ij}^2} + \frac{\vec{r}_{ik}}{r_{ik}^2}\right)\right] - \mathrm{K}(cos\beta - cos\beta_0)\left[\frac{\vec{r}_{jl}}{r_{jl}r_{ji}} - cos\beta\left(\frac{\vec{r}_{ji}}{r_{ji}^2}\right)\right] - \mathrm{K}(cos\gamma - cos\gamma_0)\left[\frac{\vec{r}_{km}}{r_{ki}r_{km}} - cos\theta\left(\frac{\vec{r}_{ki}}{r_{ki}^2}\right)\right] \quad (4)$$

where K is a force constant, α, β, γ are the current bond angles, and α_0, β_0, γ_0 is the equilibrium bond angles.[7]

$\mathrm{F}_i^{\text{adhesion}}$ represents the force of adhesion between cells and the ECM fibers. We identify the fiber nodes j within the threshold range of each cell node i, then $\mathbf{F}_i^{\text{adhesion}} = \sum_{j=1}^{N}(F_{max} - k_{ad}\mathbf{r}_{ij})$. Correspondingly, a reaction force will applied to the fiber nodes. Here, N represents the

total number of fiber nodes within the threshold range, F_{max} is the maximum adhesion force of each node, and k_{ad} represents a force constant.[16]

Table S1 The definition of parameters in the numerical model and associated values

Parameter	Definition	Value	Reference
$E_{membrane}$	Elasticity of the membrane	$9 \times 10^4\ pN/\mu m$	1
$\mu_{skeleton}$	Viscoelastic coefficients of the skeleton	$0.3\ pN\ s/\mu m$	10
$E_{skeleton}$	Elastic coefficients of the skeleton	$35\ pN/\mu m$	10
σ_c	Normal intercellular force index	$1100\ pN/\mu m^2$	1,2
τ_c	Shear intercellular force	$550\ pN/\mu m^2$	1,2
δ_0	Equilibrium distance of the intercellular interaction	$0.5\mu m$	1,2
δ_{dn}, δ_{dt}	Critical lengths of the normal and shear forces	$1\mu m$	1,2
δ_{fn}, δ_{ft}	Cutoff lengths of the interaction force	$2\mu m$	1,2
k_d	Cell contraction strength	$10\ pN/\mu m$	4,14
k_a	Area constraint constant	$5 \times 10^4\ pN/\mu m$	15
k_{dv}	Driving force strength	$1\ pN/\mu m$	1
K	Bending stiffness	$1000\ pN \cdot \mu m$	7
k_{ad}	Adhesion force constant	$20\ pN/\mu m$	16
F_{max}	Maximum adhesion force	$100\ pN$	16

Numerical simulation

The tumor spheroids – fiber matrix system was first built with given cell density and fiber density. Of course, the density of cells and fibers was adjustable and the orientation of the fibers in the network was randomly established. For instance, the choice of fiber density in the simulation is based on the measurement in our experiments. According to the fiber density in our experiment, we determined the number of fibers in our simulation model, where the fibers were randomly arranged and formed a fiber network. In this way, we were able to ensure that the fiber density and

corresponding pore size in our model were consistent with our experiments.

Prior to cell migration simulations, the cell layer underwent a short period of relaxation simulation. The simulations were conducted using a personalized FORTRAN solver. The explicit Euler method was utilized for the time propagation of the solution with a small time step to guarantee the solution stability.[1, 2] Graphical and visual analysis were performed using the Visual Molecular Dynamics (VMD) package.[17]

In the simulation of cell migration, the cells could form adhesion with (at cell front) and detach from (at cell rear) the fibers during cell migration. Corresponding to the fiber density in our experiments, the pore size in the fiber matrix is smaller than the cell size, therefore there were few chances that cells could be trapped in the empty spaces between the network without any adhesion with surrounding fibers. This is consistent with our experimental observation. Second, we used a reasonable value for the cutoff for calculating the cell-fiber interaction force in our simulation, ensuring that the cells could normally find adjacent fibers to form adhesion.

To determine the aspect ratio and angle of each cell, an ellipse was fitted to the cell shape. The least square method was utilized to fit the ellipse equation with the boundary particles' coordinates.[1, 2] Upon fitting, the central coordinates of the ellipse (x_0, y_0), the long axis radius a, the short axis radius b, and the cell angle θ between the long axis and the x-axis were obtained. Ultimately, the cell aspect ratio was calculated by dividing the long axis by the short axis of the ellipse.

The virial stress of the CG particles was calculated in order to analyze the distribution of stress throughout the cell layer:[18, 19]

$$\sigma_{\alpha\beta} = \frac{1}{\Omega}\sum_{i \text{ in } \Omega}\left[-m^{(i)}\left(u_\alpha^{(i)} - \bar{u}_\alpha\right)\left(u_\beta^{(i)} - \bar{u}_\beta\right) + \frac{1}{2}\sum_j \left(x_\alpha^{(j)} - x_\alpha^{(i)}\right) f_\beta^{(ij)}\right] \tag{5}$$

where $m^{(i)}$ denotes the mass of the ith particle in the domain Ω, $x^{(i)}$ is the position vector of particle i, with Cartesian components represented as $\left(x_\alpha^{(i)}, x_\beta^{(i)}\right) = \left(x^{(i)}, y^{(i)}\right)$. $u^{(i)}$ denotes the velocity vector of particle i, while $\bar{u}$ denotes the local average velocity of the particles in the domain Ω. Finally, $f^{(ij)}$ represents the force generated by particle j on particle i.[1, 2]

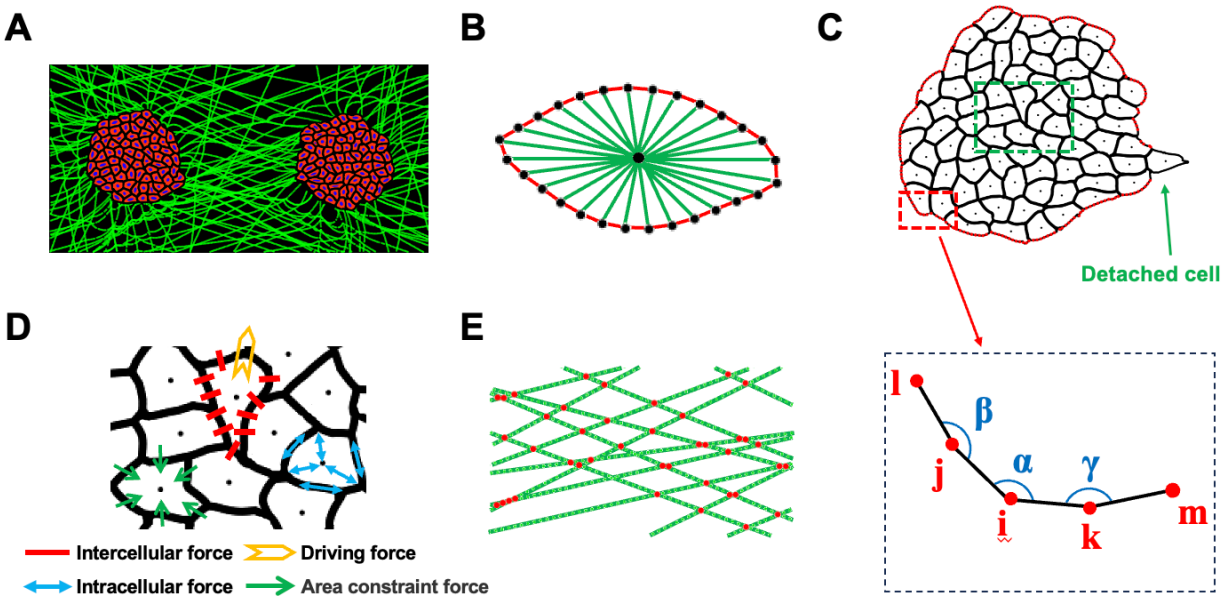

Fig. S1 Coarse-grained model of interaction between tumor spheroids and fibrous matrix. (A) Schematic illustration of the dual tumor-spheroids embedded in the fibrous matrix. The interaction between cells and ECM fibers is modeled by Lennard-Jones potential between particles on the cell and those of fibers within a threshold range. (B) CG model of a cell. The model comprises the cell membrane (black) and cytoskeleton (green). The membrane CG particles are laterally connected by springs as bonded interaction (red), while each of them is also linked to the central particle to model the cytoskeleton (green). (C) Schematic illustration of the tumor spheroid model. The cortical membrane is represented by a transcellular actin bundle-like structure at the boundary of the tumor spheroid. The boundary particles (red) are identified using the eight-quadrant method. If the number of boundary points in a single cell exceeds 50% of the total number of particles in the cell, it is considered as a detached cell. The boundary points are changed dynamically during the simulation process. The inset illustrates particle *i* and its neighboring particles *j, k, l, m* for calculating the restricting force from the basement membrane. (D) Schematic illustration of the intracellular and intercellular forces. The model considers intracellular forces (interaction within the cell), intercellular forces (attraction and repulsion between cells), cell active contractile force, cell driving force, and area constraint force. Cell active force and the random perturbation force are not shown in the figure. (E) Schematic illustration of CG model of the ECM fibrous network. The fibers are randomly arranged to form a fibrous network with a given fiber density. Each fiber consists of a series of CG particles connected by elastic springs. The fibers are connected with bonded interaction at their intersection points (red dots) to mimic the crosslink between/among them in the network. The fibers can be deformed by the forces exerted by cells through cell-fiber adhesion, while the fiber stiffening because of the deformation will, in turn, influence cell-fiber adhesion.

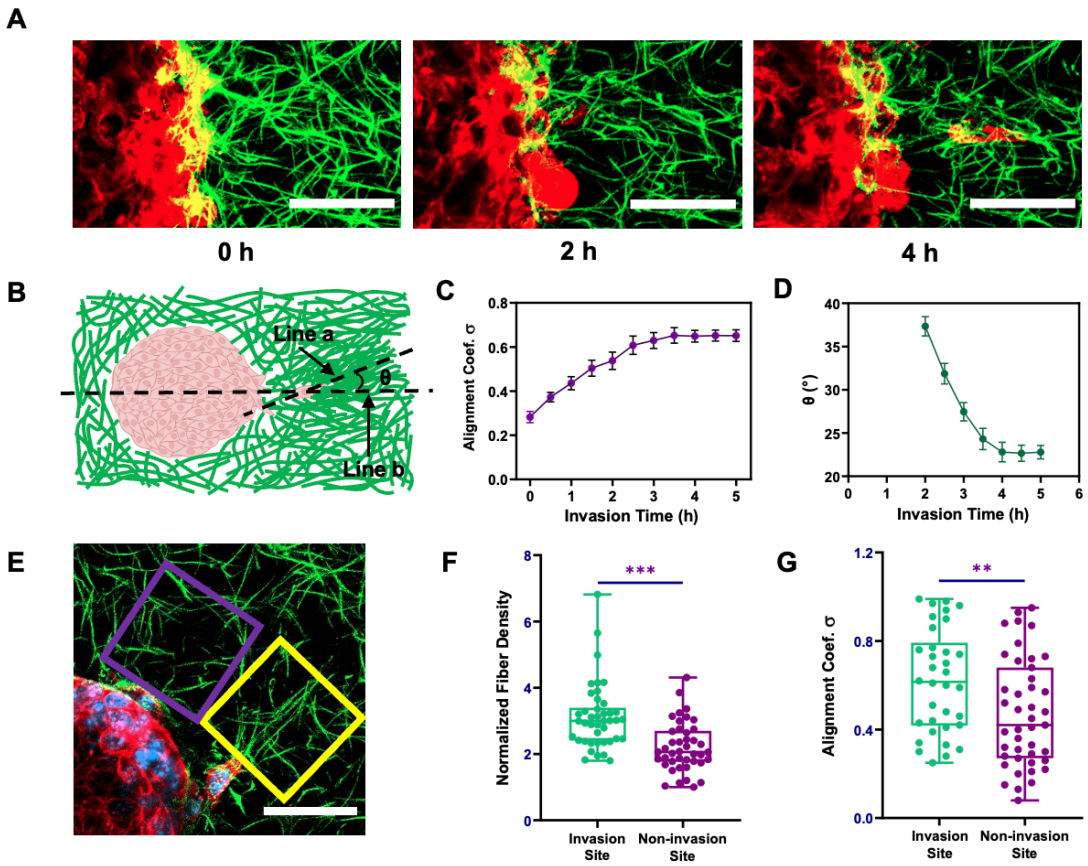

Fig. S2 The alignment and re-arrangement of fibers around the single tumor spheroid under the active contraction of cells and tissue. (A) Fluorescent images of the remodeling of fiber matrix and cell detaching from tumor spheroid at 0, 2, and 4 hours. Red represents cells, and green represents collagen fibers. The scale bar is 50 μm. (B) Schematic illustration of the arrangement of fibers around the tumor and migration direction of tumor cell. Line a indicates the direction of cell polarization, line b indicates the direction of the line connecting the center of the tumor spheroid and the cell, and θ is the angle between these two lines. (C) Relationship between collagen fiber alignment and tumor cell invasion time. (D) Relationship between θ and tumor cell invasion time. (E) Fluorescent images of the invasion and non-invasion sites at 3h. Purple boxes represent non-invasion sites, and yellow boxes represent invasion sites. Red represents cells, blue represents cell nuclei, and green represents collagen fibers. The scale bar is 50 μm. (F) Normalized fiber density in the invasion and non-invasion sites. (G) Collagen fiber alignment coefficient in the invasion and non-invasion areas. The statistical analysis of panel F and G was conducted using the one-sample t-test method.

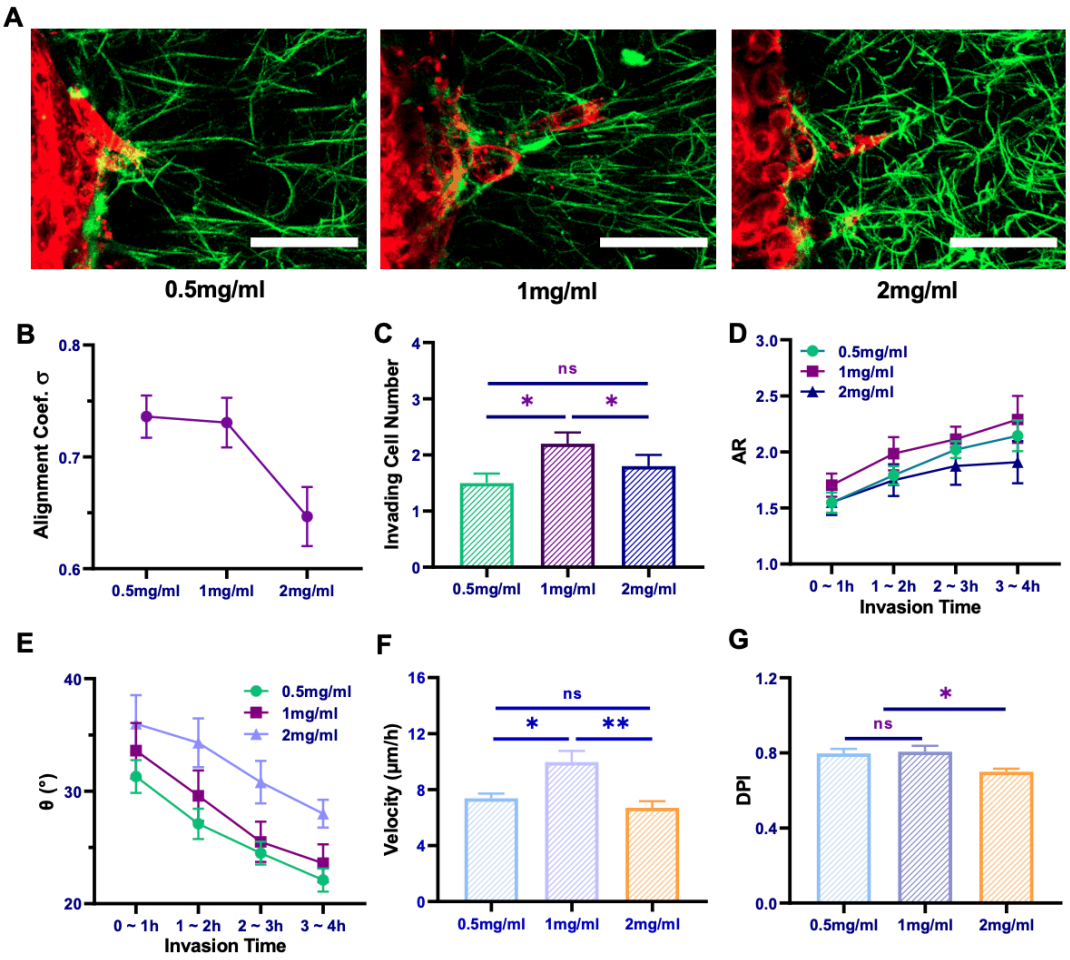

Fig. S3 Effect of collagen fiber density on tumor invasion for single tumor spheroid. (A) Representative fluorescence images of single tumor invasion for three different collagen concentrations: 0.5, 1, and 2 mg/ml. Red is for cells, and green is for collagen fiber. Scale bar, 50 μm. (B) Collagen fiber alignment near invading cells at 4 h after seeding of the tumor. (C) The number of invading cells per 100 μm arc length of tumor-spheroids over 4 h. (D) The aspect ratio of invading cells as a function of invasion time. (E) θ as a function of invasion time. (F) The average velocity of invading cells over 4 h. (G) The DPI of invading cells over 4 h. The statistical analyses in panels C, F, and G were performed using one-way ANOVA.

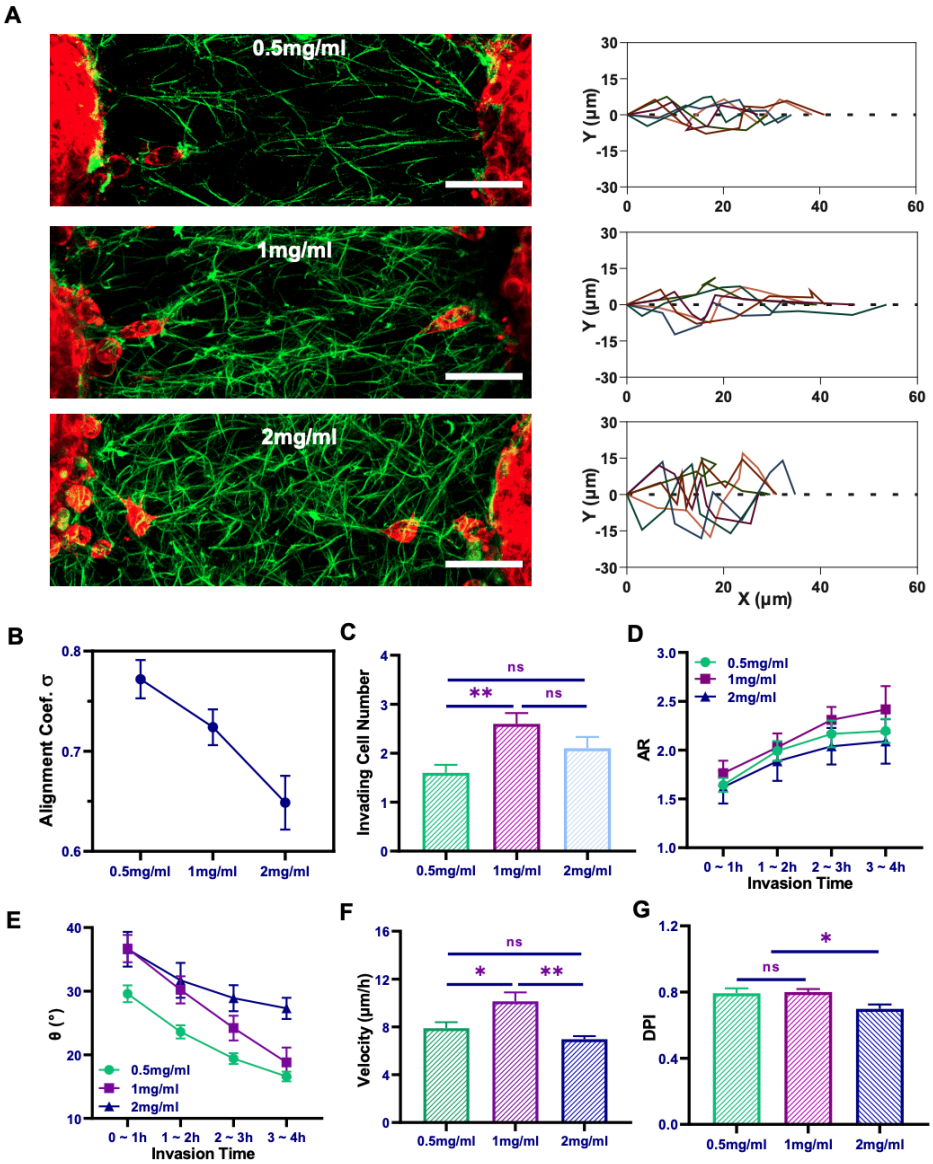

Fig. S4 Effect of collagen fiber density on tumor invasion at spheroid distance 240 μm. (A) Representative fluorescence images of tumor cell invasion into fiber matrix at various collagen concentrations: 0.5, 1, and 2 mg/ml. The right panels are the corresponding cell paths/tracks of cell invasion. Red is for cells, and green is for collagen fiber. Scale bar, 50 μm. (B) The alignment of collagen fiber in the region between the two tumor-spheroids. (C) The number of invading cells per 100 μm arc length of tumor-spheroids. (D) The aspect ratio of neighboring invading cells as a function of invasion time. (E) Cell angle θ as a function of invasion time. (F) The average velocity of neighboring invading cells over 4h. (G) The DPI of invading tumor cells over 4h. The statistical analyses in panels C, F, and G were performed using one-way ANOVA.

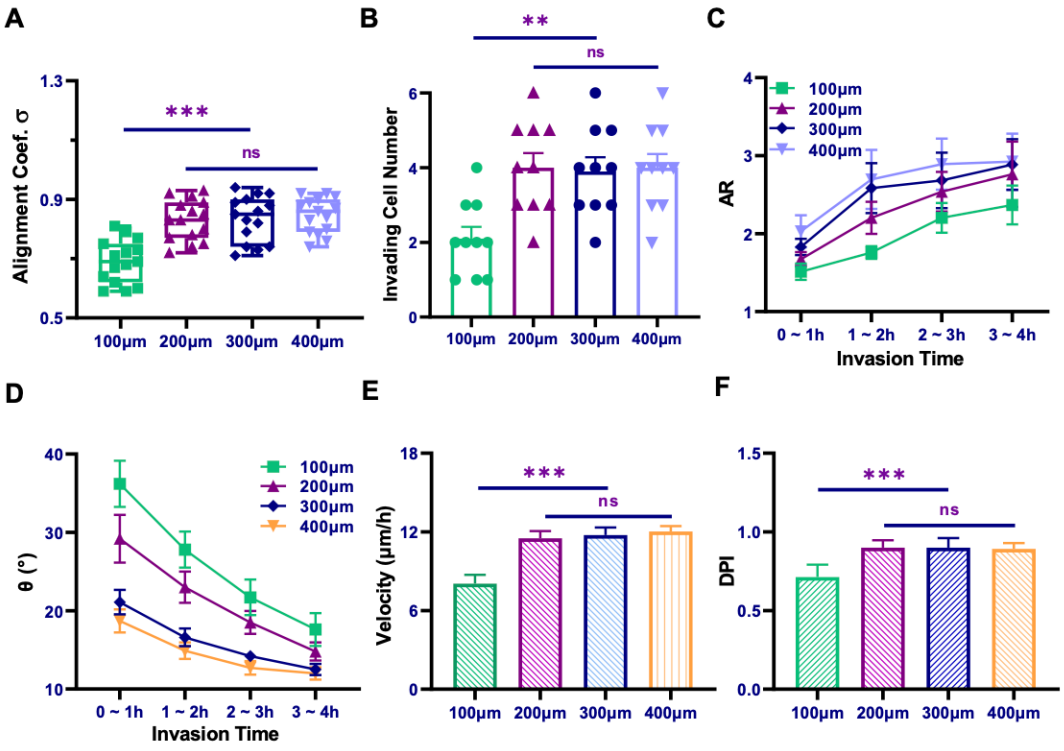

Fig. S5 Effect of tumor diameter on tumor invasion behaviors at a spheroid distance of 120 μm. (A) The alignment of the fibers in the region between the two tumor-spheroids for different spheroid diameters at t=4 h. (B) The number of invading cells per 100 μm arc length of tumor-spheroids at t=4 h. (C) The aspect ratio of invading cells as a function of invasion time. (D) Cell angle θ as a function of invasion time. (E) The average velocity of invading cells at t=4 h for different spheroid diameters. (F) The DPI of invading cells at t=4 h. The statistical analyses in panels A, B, E, and F were performed using one-way ANOVA.

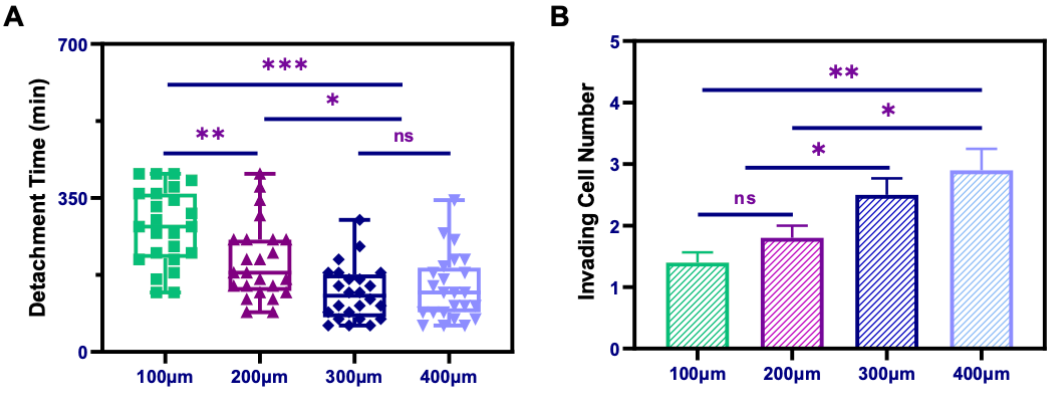

Fig. S6 Effect of tumor diameter on tumor invasion for single tumor spheroid. (A) The mean time of cell detachment from tumor-spheroids for different spheroid diameters. (B) The number of invading cells per 100 μm arc length of tumor-spheroids for different spheroid diameters at t=4 h. The statistical analyses in the figure were performed by using one-way ANOVA.

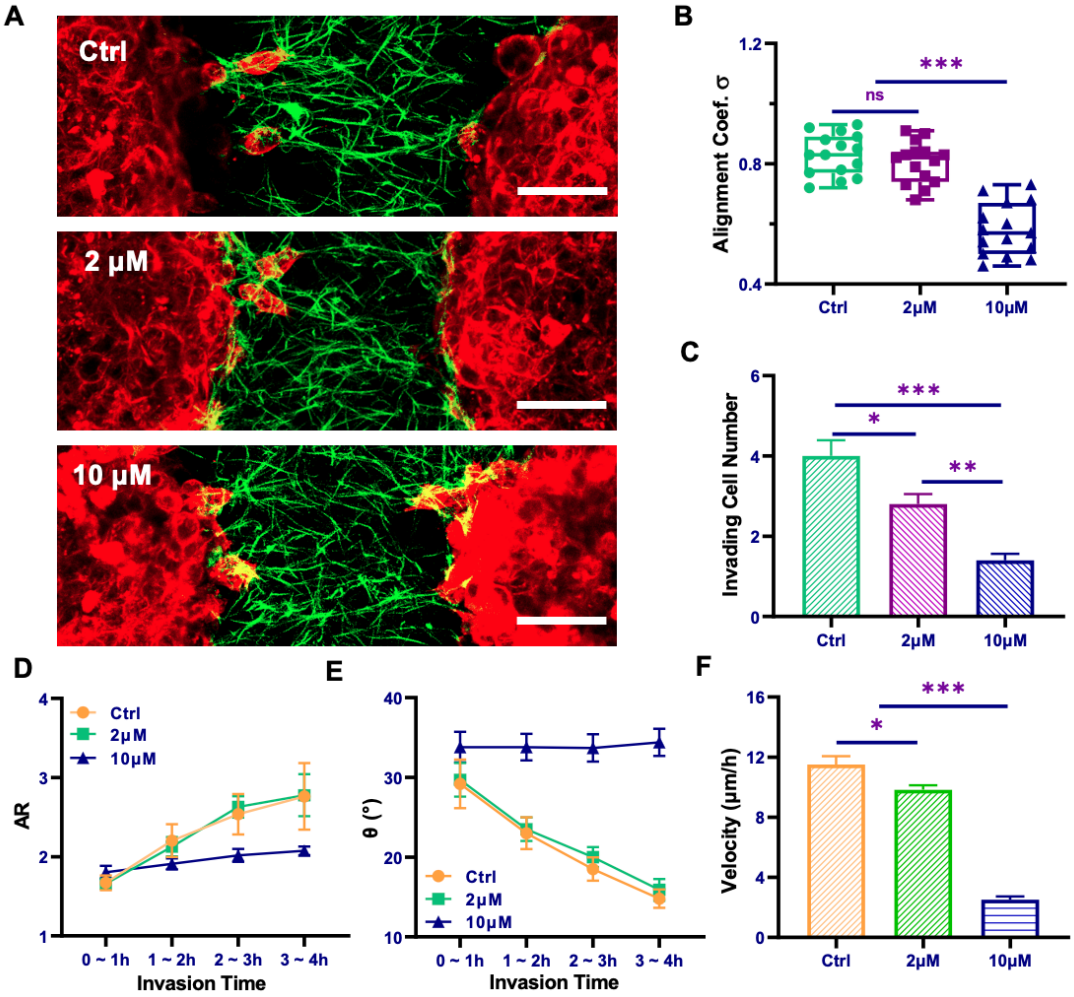

Fig. S7 Effect of cell contraction on tumor invasion behaviors for tumor spheroid distance of 120 μm. (A) Fluorescence images of tumor cell invasion after drug treatment (DMSO, 2 μM blebbistatin, and 10 μM blebbistatin) compared with control. Red is the cells, and green is collagen fiber. Scale bar, 50 μm. (B) The alignment of collagen fiber in the region between the two tumor-spheroids at t=4 h. (C) The number of invading cells per 100 μm arc length of tumor-spheroids at t=4 h. (D) The aspect ratio of invading cells as a function of invasion time. (E) Cell angle θ as a function of invasion time. (F) Effect of drug treatment on the mean velocity of invading cells. The statistical analyses in panels B, C, and F were performed using one-way ANOVA.

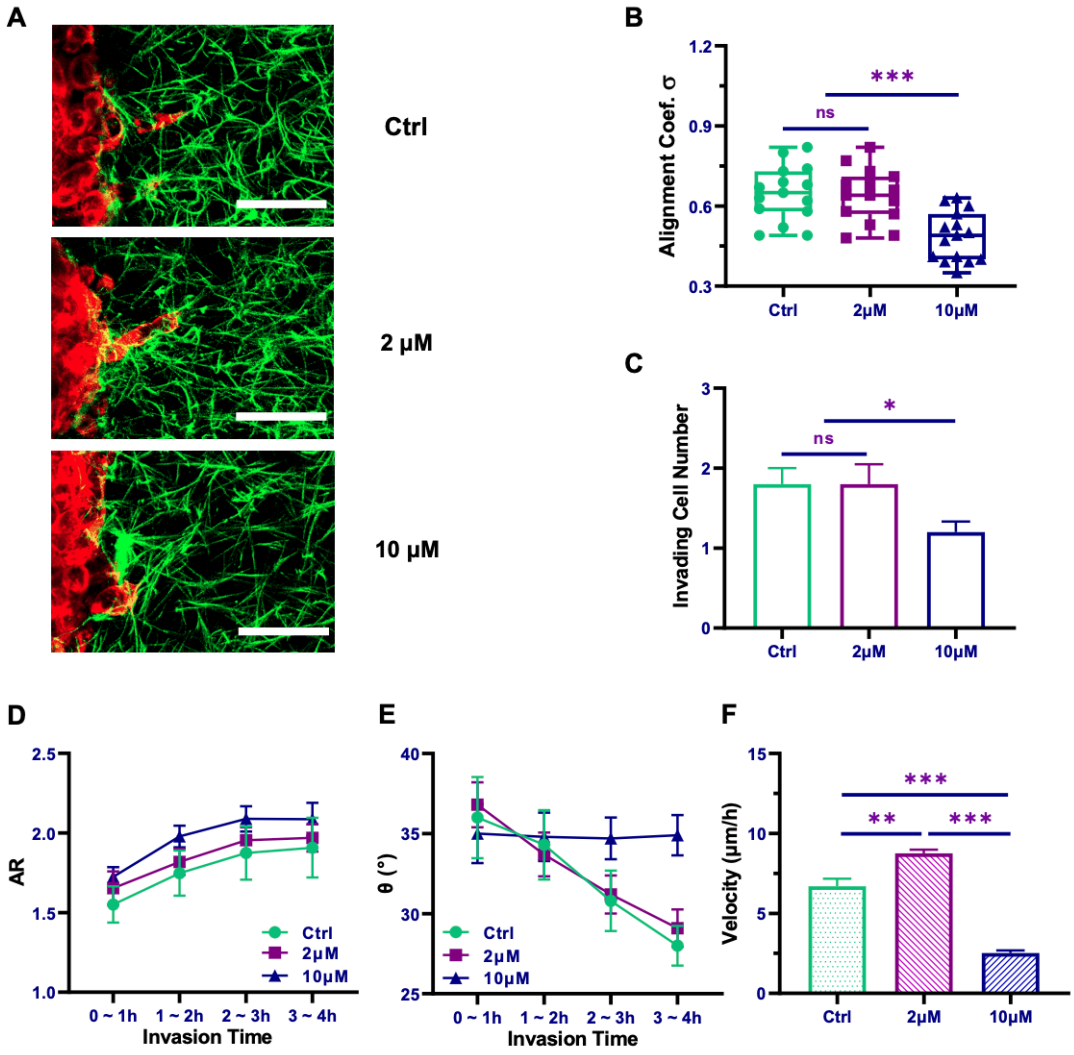

Fig. S8 Effect of cell contraction on tumor cell invasion for single tumor spheroid. (A) Fluorescence images of tumor invasion after drug treatment (DMSO, 2 μM blebbistatin, and 10 μM blebbistatin) compared with control. Red is the cells, and green is collagen fiber. Scale bar, 50 μm. (B) The alignment of collagen fiber near tumor spheroid at t=4 h. (C) The number of invading cells per 100 μm arc length of tumor-spheroids at t=4 h. (D) The aspect ratio of invading cells as a function of invasion time. (E) Cell angle θ as a function of invasion time. (F) The mean velocity of invading cells for different treating conditions. The statistical analyses in panels B, C, and F were performed using one-way ANOVA.

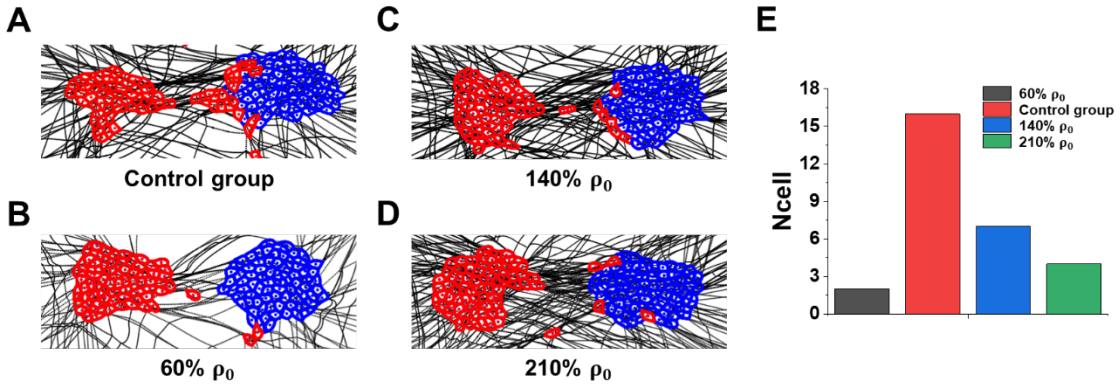

Fig. S9 The non-monotonic relationship between the number of invading cells and fiber density. The number of cells was highest at ρ_0 (A), but when the fiber density decreases to 60%ρ_0 (B) or increases to 140%ρ_0 (C) and 210% ρ_0 (D), the number of invasive tumor cells became lower.

References

1. X. Xu, J. Xu, X. Li, J. Song, D. Li and B. Ji, *J. Appl. Mech-T. ASME*, 2022, **89**, 051005.
2. J. Xu, X. Xu, X. Li, S. He, D. Li and B. Ji, *Biophys. J.*, 2022, **121**, 288-299.
3. Y. Zhong and B. Ji, *Eur. Phys. J. Spec. Top.*, 2014, **223**, 1373-1390.
4. S. He, Y. Su, B. Ji and H. Gao, *J Mech Phys Solids*, 2014, **70**, 116-135.
5. U. S. Schwarz and S. A. Safran, *Phys. Rev. Lett.*, 2002, **88**, 048102.
6. K. Mandal, I. Wang, E. Vitiello, L. A. C. Orellana and M. Balland, *Nat. Commun.*, 2014, **5**, 5749.
7. H. Tang, D. Laporte and D. Vavylonis, *Mol. Biol. Cell*, 2014, **25**, 3006-3016.
8. J. K. Klarlund, *Proc. Natl. Acad. Sci.*, 2012, **109**, 15799-15804.
9. T. Chen, A. Callan-Jones, E. Fedorov, A. Ravasio, A. Brugués, H. T. Ong, Y. Toyama, B. C. Low, X. Trepat and T. Shemesh, *Nat Phys*, 2019, **15**, 393-402.
10. I. V. Dokukina and M. E. Gracheva, *Biophys. J.*, 2010, **98**, 2794-2803.
11. L. Q. Lin and X. W. Zeng, *Biomech. Model. Mechanobiol.*, 2018, **17**, 439-448.
12. X. Trepat and J. J. Fredberg, *Trends Cell Biol.*, 2011, **21**, 638-646.
13. Z. J. Liu, J. L. Tan, D. M. Cohen, M. T. Yang, N. J. Sniadecki, S. A. Ruiz, C. M. Nelson and C. S. Chen, *Proc. Natl. Acad. Sci. U.S.A.*, 2010, **107**, 9944-9949.
14. J. Stricker, Y. Aratyn-Schaus, P. W. Oakes and M. L. Gardel, *Biophys. J.*, 2011, **100**, 2883-2893.
15. S. Koride, A. J. Loza and S. X. Sun, *APL Bioeng.*, 2018, **2**, 031906.
16. S. V. Plotnikov, A. M. Pasapera, B. Sabass and C. M. Waterman, *Cell*, 2012, **151**, 1513-1527.
17. W. Humphrey, A. Dalke and K. Schulten, *J. Mol. Graph. Model.*, 1996, **14**, 33-38.

18. A. K. Subramaniyan and C. T. Sun, *Int J Solids Struct*, 2008, **45**, 4340-4346.
19. J. Cormier, J. M. Rickman and T. J. Delph, *J. Appl. Phys.*, 2001, **89**, 99-104.